

Surface Plasmon Polaritons on Metallic Surfaces

Masud Mansuripur, Armis R. Zakharian and Jerome V. Moloney

Recent advances in nano-fabrication have enabled a host of nano-photonics experiments involving subwavelength metallic structures. This flurry of activity has, in turn, reawakened interest in surface plasmon polaritons (SPPs) and inspired theoretical research in this area. Although the fundamental properties of SPPs have been known for nearly five decades, there remain certain subtle issues that could benefit from further critical analysis. Here, numerical simulations are used to verify the detailed structure of long-range SPPs.

We present field distribution profiles and energy flow patterns aimed at promoting a physical understanding of SPP generation and propagation in ways that mathematical equations alone cannot convey. Thus, beginning with Maxwell's equations, we determine the electromagnetic eigenmodes confined to flat metallo-dielectric interfaces. The behavior of these modes will then be examined through computer simulations that show the excitation of SPPs in certain practical settings. Our numerical computations are based on the Finite Difference Time Domain (FDTD) method.

With reference to Fig. 1, in a homogeneous medium of dielectric constant ϵ the propagation vector is $\mathbf{k} = k_0(\sigma_y \hat{\mathbf{y}} + \sigma_z \hat{\mathbf{z}})$, where $k_0 = 2\pi/\lambda_0$ and $\sigma_y^2 + \sigma_z^2 = \epsilon$. In general, $\sigma_z = \pm\sqrt{\epsilon - \sigma_y^2}$, with both plus and minus signs admissible. In each of the semi-infinite cladding media, however, only one value of σ_z is allowed, corresponding to the solution that approaches zero when $z \rightarrow \pm\infty$. This is why σ_{z1} of the upper cladding in Fig. 1 is chosen to have a plus sign, whereas that of the lower

cladding has a minus sign. (σ_{z1}, σ_{z2} have positive imaginary parts.)

The E - and H -fields of each plane-wave are related through the Maxwell equation $\nabla \times \mathbf{H} = \partial \mathbf{D} / \partial t$ (where $\mathbf{D} = \epsilon_0 \epsilon \mathbf{E}$) as follows:

$$H_x(y, z, t) = H_0 \exp\{i[k_0(\sigma_y y \pm \sigma_z z) - \omega t]\} \quad (1a)$$

$$E_y(y, z, t) = \mp(Z_0 \sigma_z / \epsilon) H_x(y, z, t) \quad (1b)$$

$$E_z(y, z, t) = (Z_0 \sigma_y / \epsilon) H_x(y, z, t) \quad (1c)$$

Here, H_0 is the (complex) amplitude of the magnetic field, $Z_0 = \sqrt{\mu_0 / \epsilon_0} \approx 377 \Omega$ is the impedance of the free space, and $\omega = k_0 c = k_0 \sqrt{\mu_0 \epsilon_0}$ is the temporal frequency of the light wave. The time-dependence factor $\exp(-i\omega t)$ shall be omitted in the following discussion. We confine our attention to symmetric structures where both cladding media have the same dielectric constant ϵ_1 . In general, the modal fields are either odd or even with respect to the y -axis, allowing one to express the H -field

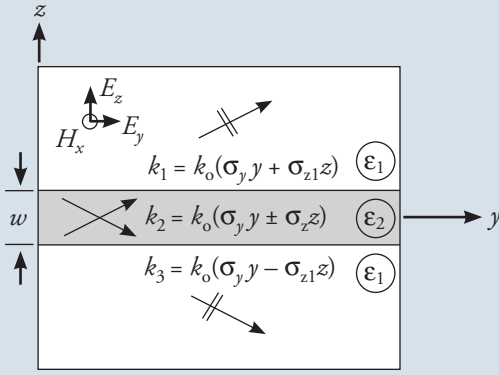


Figure 1. Slab of thickness w and dielectric constant ϵ_2 , sandwiched between two homogeneous, semi-infinite media of dielectric constant ϵ_1 . An electromagnetic mode of the structure consists of two (generally inhomogeneous) plane-waves within the slab and a single (inhomogeneous) plane-wave in each of the surrounding media. Continuity of the fields at $z = \pm 1/2w$ requires that $k_y = k_0\sigma_y$ be the same for all these plane-waves. Although the polarization state of the mode can generally be either TE or TM, only TM modes are considered in this article. The magnetic field, therefore, has a single component H_x along the x -axis, while the electric field has two components (E_y, E_z) in the yz -plane. Throughout the article, $\lambda_0 = 650$ nm and the metallic medium is silver, having $\epsilon = -19.6224 + 0.443i$ (corresponding to $n + ik = 0.05 + 4.43i$).

of a given mode as follows (\pm signs for even and odd modes, respectively):

$$H_x(y, z) = \begin{cases} H_1 \exp(ik_0\sigma_y y) \exp[ik_0\sigma_{z1}(z - 1/2w)]; & z \geq +1/2w \\ H_2 \exp(ik_0\sigma_y y) [\exp(ik_0\sigma_{z2} z) \\ \pm \exp(-ik_0\sigma_{z2} z)]; & |z| \leq 1/2w \\ \pm H_1 \exp(ik_0\sigma_y y) \exp[-ik_0\sigma_{z1}(z + 1/2w)]; & z \leq -1/2w \end{cases} \quad (2)$$

The corresponding E -field for each mode can be found from Eqs. (1). Continuity of H_x and E_y at the $z = \pm 1/2w$ boundaries yields:

$$H_2 [\exp(ik_0\sigma_{z2} w/2) \pm \exp(-ik_0\sigma_{z2} w/2)] = H_1 \quad (3a)$$

$$Z_0 H_2 (\sigma_{z2}/\epsilon_2) [\exp(ik_0\sigma_{z2} w/2) \mp \exp(-ik_0\sigma_{z2} w/2)] = Z_0 H_1 (\sigma_{z1}/\epsilon_1) \quad (3b)$$

Substituting for H_1 from Eq. (3a) into Eq. (3b), rearranging the terms, and expressing σ_{z1} and σ_{z2} in terms of σ_y , we find:

$$\frac{\epsilon_1 \sqrt{\epsilon_2 - \sigma_y^2} - \epsilon_2 \sqrt{\epsilon_1 - \sigma_y^2}}{\epsilon_1 \sqrt{\epsilon_2 - \sigma_y^2} + \epsilon_2 \sqrt{\epsilon_1 - \sigma_y^2}} \exp(ik_0 \sqrt{\epsilon_2 - \sigma_y^2} w) = \pm 1 \quad (4)$$

This transcendental equation in $\sigma_y = \sigma_y^{(r)} + i\sigma_y^{(i)}$ is the characteristic equation of the waveguide depicted in Fig. 1. Each solution σ_y of Eq. (4) corresponds to a particular mode of the waveguide; when the plus (minus) sign is used on the right-hand side of Eq. (4), the solution represents an even (odd) mode. Since we are interested in modes that propagate from left to right, the imaginary part of σ_y must be non-negative (i.e., $\sigma_y^{(i)} \geq 0$). Otherwise the mode will grow exponentially as $y \rightarrow \infty$. Also, when computing the complex square roots in Eq. (4), one must always choose the root that has a positive imaginary part.

Note that the coefficient multiplying the complex exponential on the left-hand side of Eq. (4) is the Fresnel reflection coefficient r_p for a p -polarized (TM) plane-wave at the interface between media of dielectric constants ϵ_1 and ϵ_2 . The Fresnel coefficient has a singularity (pole) at $\sigma_y = \sqrt{\epsilon_1 \epsilon_2 / (\epsilon_1 + \epsilon_2)}$, where

its denominator vanishes. The function on the left-hand side of Eq. (4) thus varies rapidly in the vicinity of this pole, where some of the solutions of the equation are to be found. In particular, when $w \rightarrow \infty$, the complex exponential approaches zero and the pole itself becomes a solution. This can be seen most readily with reference to Eqs. (3); by allowing $\exp(+ik_0\sigma_{z2} w/2) \rightarrow 0$ and substituting for H_1 from Eq. (3a) into Eq. (3b), we find $\sigma_{z2}/\epsilon_2 = -\sigma_{z1}/\epsilon_1$, namely, $\epsilon_1 \sqrt{\epsilon_2 - \sigma_y^2} + \epsilon_2 \sqrt{\epsilon_1 - \sigma_y^2} = 0$.

Metallic slab in the free space

Consider the case of $\epsilon_1 = 1.0$, $\epsilon_2 = -19.6224 + 0.443i$ (silver at $\lambda_0 = 650$ nm). Fixing the slab's thickness at $w = 50$ nm and searching the complex-plane for solutions of Eq. (4) yields the first few values of $\sigma_y^{(\pm)} = \sigma_y^{(r)} + i\sigma_y^{(i)}$ listed in Table 1; the \pm superscripts identify the even and odd modes, respectively. (Only solutions having non-negative values of $\sigma_y^{(i)}$ are considered so that, as $y \rightarrow +\infty$, the corresponding modes will decay to zero.) Although we will be concerned mainly with the top two (fundamental) solutions, there exists an infinite number of solutions with large values of $\sigma_y^{(i)}$. The latter are generally needed to match the boundary conditions upon launching an SPP; otherwise, due to their rapid decay along the y -axis, modes with large $\sigma_y^{(i)}$ do not appear to have any practical significance.

As the slab thickness w increases, the fundamental solutions (highlighted in Table 1) approach each other, reaching the common value of $\sigma_{\text{spp}} = \sqrt{\epsilon_1 \epsilon_2 / (\epsilon_1 + \epsilon_2)} = (1.0265 + i 0.6217 \times 10^{-3})$. In contrast, reducing the slab thickness causes the fundamental solutions to move apart (and also further away

$\sigma_y^{(+)}$	$\sigma_y^{(-)}$
1.017 + i 0.22 × 10 ⁻³	1.041 + i 1.39 × 10 ⁻³
0.171 + i 7.868	0.204 + i 13.738
-0.1145 + i 7.860	-0.1722 + i 13.729
0.211 + i 20.0012	0.2135 + i 26.3795
-0.1892 + i 19.992	-0.1965 + i 26.3698

Table 1. First few solutions of Eq. (4) for a 50 nm-thick silver slab ($\lambda_0 = 650$ nm, $\epsilon_1 = 1.0$, $\epsilon_2 = -19.6224 + 0.443i$)

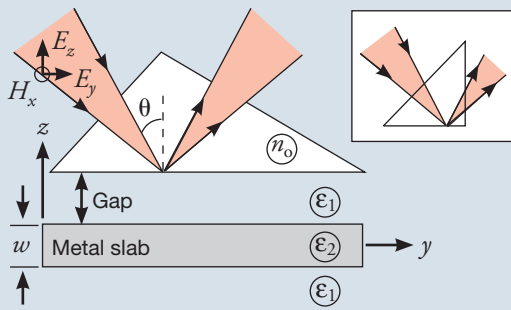


Figure 2. A Gaussian beam of wavelength λ_o is focused at the bottom of a glass prism of refractive index n_o . The angle of incidence θ is slightly greater than the critical angle θ_c of total internal reflection. (In this two-dimensional system, the beam is focused by a cylindrical lens; its shape, therefore, does not vary along the x -axis.) The beam is linearly polarized, with H -field along x and E -field components (E_y, E_z) confined to the plane of incidence. A small gap separates a metallic slab of thickness w and dielectric constant ϵ_2 from the prism; the medium immediately above and below the slab has dielectric constant ϵ_1 . The inset shows a half-prism that can be used to eliminate the back-coupling of the surface plasmon(s), excited on the metallic surface(s), into the prism.

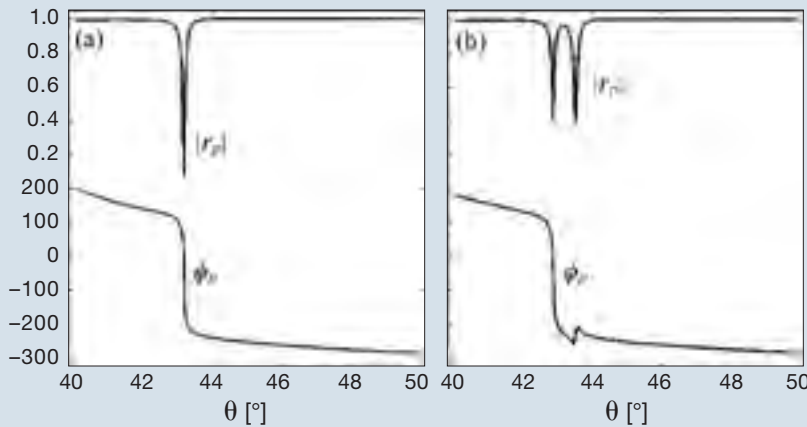


Figure 3. Plots of the Fresnel reflection coefficient for p -polarized (TM) light, $r_p = |r_p| \exp(i\phi_p)$, versus the incidence angle θ at the bottom of the prism of Fig. 2; $\lambda_o = 650$ nm, $n_o = 1.5$. (a) Thick silver slab separated from the prism by a 1078-nm air gap. (b) A 65 nm-thick silver slab separated by a 950 nm air gap. In each case, the gap is optimized to enhance the strength of the excited plasmon(s).

from σ_{sp}). As $w \rightarrow 0$, the even solution approaches $\sigma_y = \sqrt{\epsilon_1}$, while the odd solution acquires a large $\sigma_y^{(i)}$ and a fairly large $\sigma_y^{(o)}$. Table 2 lists the fundamental solutions of Eq. (4) for a range of values of w .

Prism-coupling

To excite SPPs on the flat surface of a metal slab, one may use the prism-coupling scheme in Fig. 2, commonly referred to as the Kretschmann or Otto configuration, depending on whether the metal is thin or thick. The incident beam arrives at the bottom of the prism (refractive index = n_o) at an angle θ which is slightly greater than the critical angle θ_c of total internal reflection. Since $k_y = k_o n_o \sin\theta$, the waves coupled to the metal slab will have $k_y > k_o$, a basic requirement for SPP excitation. The

w (nm)	$\sigma_y^{(+)}$	$\sigma_y^{(-)}$
5	$1.0003 + i 0.7 \times 10^{-6}$	$2.3422 + i 0.0432$
10	$1.0012 + i 3.7 \times 10^{-6}$	$1.4657 + i 0.01745$
50	$1.017 + i 0.22 \times 10^{-3}$	$1.041 + i 1.39 \times 10^{-3}$
65	$1.021 + i 0.35 \times 10^{-3}$	$1.033 + i 1.01 \times 10^{-3}$
200	$1.02647 + i 0.62 \times 10^{-3}$	$1.02650 + i 0.6235 \times 10^{-3}$
∞	$1.02648 + i 0.6219 \times 10^{-3}$	$1.02648 + i 0.6219 \times 10^{-3}$

Table 2. Fundamental modes of silver slabs of differing thickness ($\lambda_o = 650$ nm, $\epsilon_1 = 1.0$, $\epsilon_2 = -19.6224 + 0.443i$)

incident beam, being mildly focused, has a k -space spectrum that spans a few degrees around θ_c . Most of these k -vectors are reflected at the prism's base; however, a narrow range of incidence angles evanescently couples to the metal surface and proceeds to excite the plasmons.

Figure 3 shows computed plots of the Fresnel reflection coefficient $r_p = |r_p| \exp(i\phi_p)$ for a p -polarized plane-wave versus the incidence angle θ at the bottom of the prism ($n_o = 1.5$, $\lambda_o = 650$ nm). In Fig. 3(a), corresponding to the case of a thick silver slab separated by a 1078-nm air gap, there is a single resonant absorption at $\theta = 43.15^\circ$. Due to the narrow range of k -vectors that cross the gap, we expect the footprint of the beam on the metal surface to be much wider than the diameter of the focused spot at the prism's base. The rapid variation of the phase ϕ_p in the vicinity of the resonance implies that the footprint on the metal surface will *not* be centered under the incident spot. Rather, it will be shifted to the right.

Figure 3(b), corresponding to a 65-nm-thick silver slab separated from the prism by a 950-nm air gap, exhibits two resonant absorptions, representing the odd and even modes of the metallic slab. The first resonance at $\theta_1 = 42.86^\circ$, having the smaller value of k_y , excites the even mode, while the second resonance, at $\theta_2 = 43.52^\circ$, excites the odd mode.

The coupling of a focused beam of light through a glass prism to a thick (semi-infinite) silver slab is depicted in Figs. 4 and 5. At the base of the prism, the Gaussian beam's full-

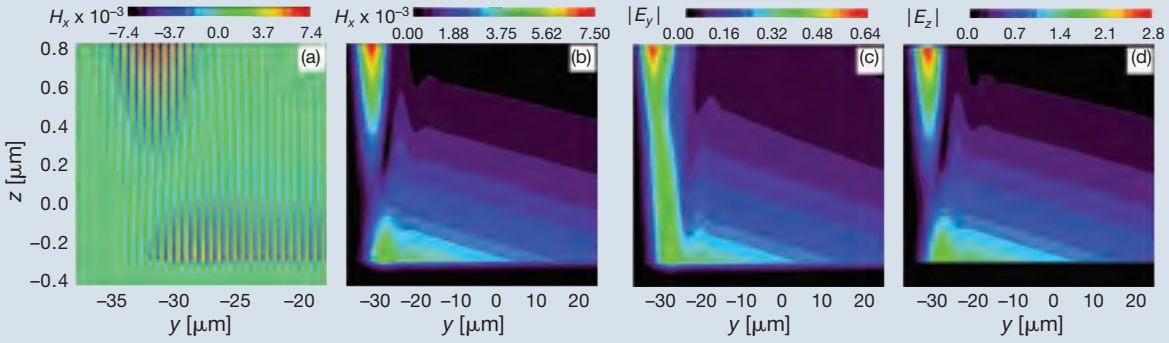


Figure 4. Electromagnetic fields in the gap region between the prism and the semi-infinite metal surface. (a) Instantaneous H_x . (b-d) Magnitudes of H_x , E_y , E_z . The evanescent field at the bottom of the prism is visible in the upper left-hand corner of each frame. The SPP is launched at the lower left-hand side. Due to back-coupling to the prism, the SPP's decay rate along the y -axis is nearly twice the expected rate.

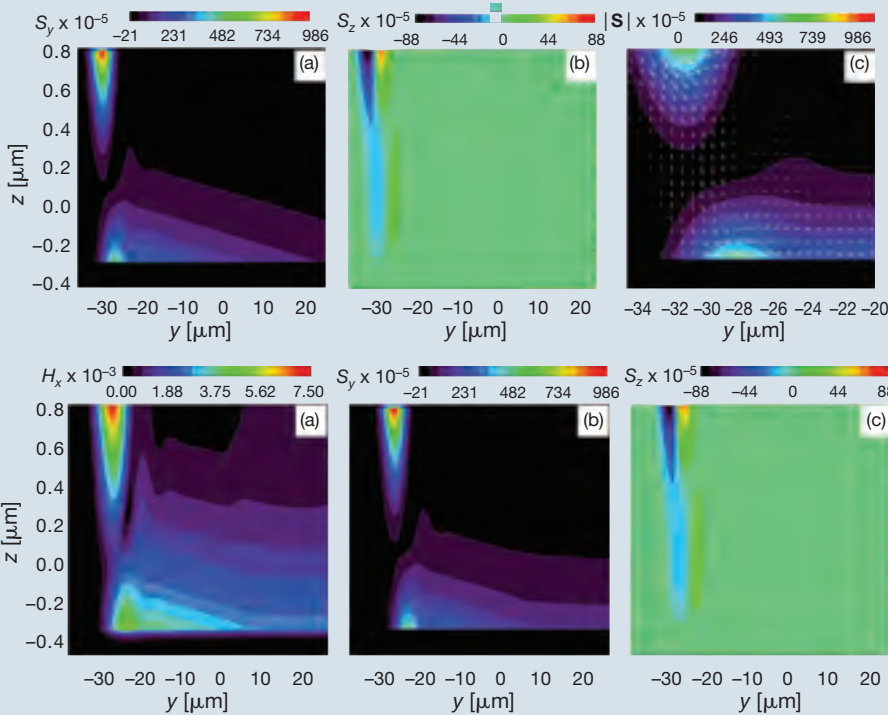


Figure 5. (a, b) Components S_y and S_z of the Poynting vector \mathbf{S} in the gap region between the prism and the semi-infinite metal. (c) Close-up of $|\mathbf{S}|$; superimposed arrows show the direction of \mathbf{S} .

Figure 6. (a-c) Plots of H_x , S_y , S_z in the gap region between the prism and a semi-infinite metallic medium. To eliminate the back-coupling of the SPP to the prism, the part of the prism that lies above the launched SPP has been removed (see the inset in Fig. 2); the prism thus extends from $-40\mu\text{m}$ to 0 along the y -axis. The SPP's decay rate along y now agrees with the theoretical prediction.

width-at-half-maximum-amplitude (FWHM) is $4.0\ \mu\text{m}$, the central ray's incidence angle is $\theta = 43^\circ$, and the air gap is $1.078\ \mu\text{m}$. The expected SPP wavelength, $\lambda_o/\text{Re}[\sigma_{\text{spp}}] = 633.22\ \text{nm}$, is consistent with $\lambda_o/(n_o \sin\theta) = 633.6\ \text{nm}$ estimated from Fig. 3(a) at the minimum of $r_p(\theta)$. From Fig. 4(a), the profile of $H_x(y)$ sampled at $\Delta z = 10\ \text{nm}$ below the metal surface, has a period of $634\ \text{nm}$ (peak of the function's Fourier spectrum), in excellent agreement with the theory.

The Poynting vector plots of Fig. 5 show how a fraction of the evanescent field's energy reaches the metal surface, of which fraction a certain portion immediately returns to the prism, while the remainder turns around and propagates along the metal surface in the y -direction.

The best fit to $\text{Re}[H_x]$ of Fig. 4(a) is $\exp(-0.01367 y) \sin [9.9165(y + 0.245)]$. While $k_o \text{Re}[\sigma_{\text{spp}}] = 9.9226$ is quite close to the observed value of 9.9165 , the decay rate of 0.01367 is substantially greater than the SPP extinction rate of $k_o \text{Im}[\sigma_{\text{spp}}] = 0.006$; this is caused by the SPP's back-coupling to the prism. We truncated the simulated prism by removing the glass that lies directly above the excited SPP (see Fig. 2, inset); the truncated prism thus occupied only the interval $(-40\ \mu\text{m}, 0)$ along the y -axis. The simulation results for the truncated prism, shown in Fig. 6, exhibit a period of $634\ \text{nm}$ in the $y \geq 0$ region (obtained from the waveform's Fourier spectrum). The best fit to $\text{Re}[H_x]$, namely, $\exp(-0.006 y) \sin [9.9165(y + 0.056)]$, now yields the expected decay rate as well.

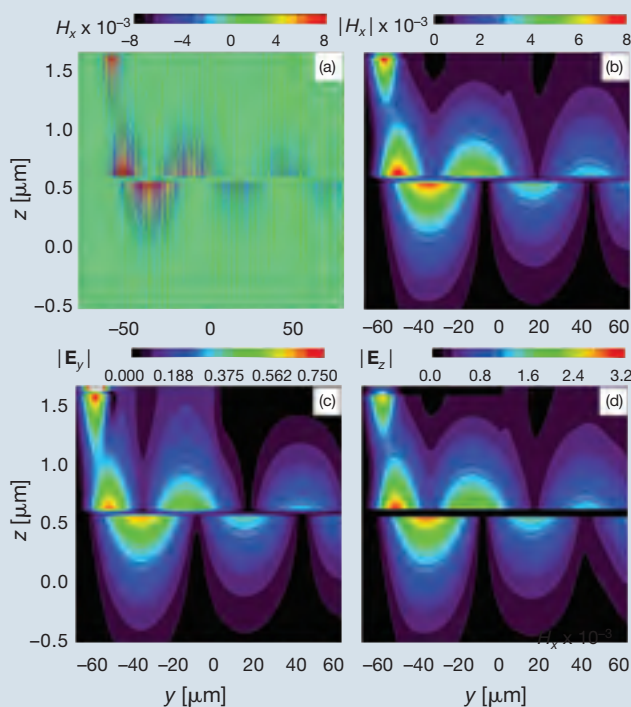


Figure 7. Electromagnetic field profiles on both sides of a 65-nm-thick silver slab illuminated through a truncated prism; the slab is centered at $z = 0.6 \mu\text{m}$, while the prism's base at $z = 1.55 \mu\text{m}$ extends from $-80 \mu\text{m}$ to 0 along the y -axis. (a) Profile of instantaneous H_x . (b-d) Magnitudes of H_x , E_y , E_z . The evanescent field just below the prism appears in the upper left-hand corner of each frame. Both odd and even modes of the slab are excited, their interference causing the peaks and valleys of the field distributions.

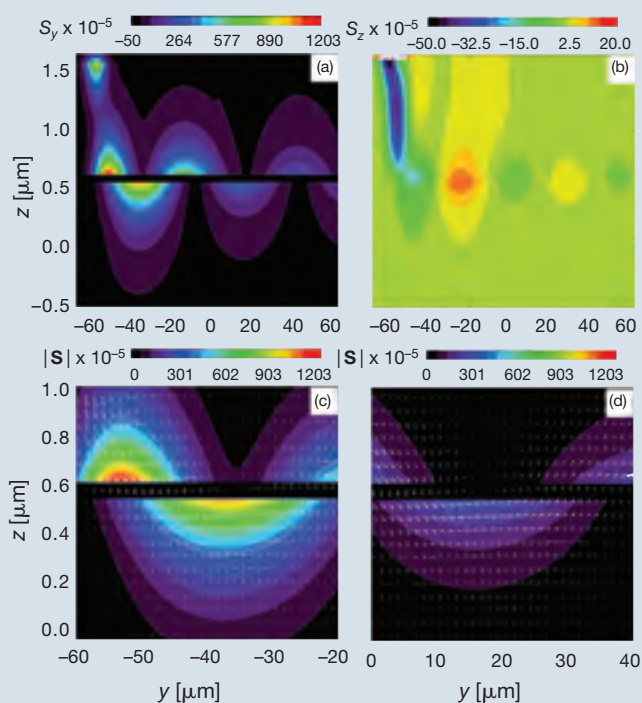


Figure 8. (a, b) Poynting vector components S_y , S_z around the 65 nm-thick silver slab illuminated through a truncated prism. (c, d) Close-ups of $|\mathbf{S}|$, showing the flow of energy in the early and late parts of the propagating SPP.

Interference between odd and even modes

Figures 7 and 8 show the results of FDTD simulations pertaining to a Gaussian beam (FWHM at prism's base = $8.0 \mu\text{m}$, $\lambda_o = 650 \text{ nm}$, $\theta = 43.55^\circ$), coupled through a truncated prism ($n_o = 1.5$, $y = -80 \mu\text{m}$ to 0 , air gap = 950 nm) to a 65-nm-thick silver slab. The Fourier transform of $\text{Re}[H_x(y)]$, sampled at $\Delta z = 10 \text{ nm}$ below the slab, yields $\lambda_{y1} = 636.9 \text{ nm}$, $\lambda_{y2} = 629.4 \text{ nm}$, in excellent agreement with $\lambda_o / (n_o \sin \theta_{1,2}) = 637.1 \text{ nm}$, 629.3 nm obtained from the minima of $r_p(\theta)$ of Fig. 3(b). Computed values of σ_y for a 65-nm-thick slab in Table 2 yield $\lambda_y^{(\pm)} = \lambda_o / \text{Re}[\sigma_y^{(\pm)}] = 636.6 \text{ nm}$, 629.2 nm , and $k_o \text{Im}[\sigma_y^{(\pm)}] = 0.0034$, 0.0098 , once again in agreement with the simulated profile of $\text{Re}[H_x(y)]$ shown in Fig. 7(a).

Profiles of the Poynting vector \mathbf{S} in the gap region between the silver slab and the prism and also in the region immediately below the slab are shown in Fig. 8. The S_z plot shows a fraction of the evanescent field's energy reaching the metal slab, of which a certain proportion immediately returns to the prism, while the remainder turns around and straddles the slab along the y -axis.

In general, the odd mode, being lossier than the even mode, has a shorter propagation distance along the y -axis. The physics behind the loss mechanism may be understood as follows. With the even mode, the field component E_z has the same sign above and below the slab; therefore, at a given point along y , the electrical charges at the top and bottom surfaces have opposite signs. Inside the metallic slab, the field component E_z —reduced by a factor of ϵ_2/ϵ_1 relative to the E_z immediately outside—helps move the charges back and forth between the top and bottom surfaces. The slab being thin, the transport distance is short; hence the charge velocity and the corresponding electrical current are small.

In contrast, the charges of the odd mode have the same sign on opposite sides of the slab. Consequently, positive and negative charges must move laterally (in the $\pm y$ -directions) during each period of oscillation. The travel distance is now on the order of the SPP wavelength, which is typically greater than the slab thickness. Therefore, the current densities of the odd mode are relatively large, leading to correspondingly large losses.

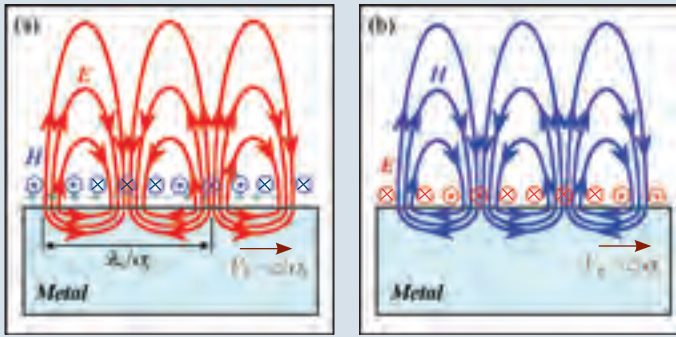


Figure 9. (a) The SPP's E -fields originate on positive charges and terminate on negative ones. Continuity of H_{\parallel} and a negative ϵ_{metal} ensure the continuity of D_{\perp} , while E_{\parallel} becomes continuous when $\sigma_y = \sigma_{\text{spp}}$. (b) A physical impossibility, since the divergence-free nature of the H -field requires H_{\parallel} to have opposite directions above and below the surface, thus prohibiting the continuity of H_{\parallel} at the boundary.

Polarization dependence of SPP

A mathematical analysis similar to the one that led to Eq. (4) reveals that TE-polarized electromagnetic waves *cannot* support SPPs at metal-dielectric interfaces. The following argument proves the same point by appealing to the underlying physics of surface plasmons. For the sake of simplicity, consider a thick metal plate in vacuum, as shown in Fig. 9. An SPP consists of two inhomogeneous plane-waves (one in the free space, the other in the metal), both having the same σ_y in the propagation direction (phase velocity $V_p = c/\sigma_y$). The diagram in Fig. 9(a) represents a true SPP, with the E -fields originating on positive (surface) charges and terminating on negative ones. If the continuity of H_{\parallel} at the surface is assumed, then a negative ϵ_{metal} ensures the continuity of D_{\perp} , and E_{\parallel} can be made continuous by the proper choice of σ_y , namely, $\sigma_y = \sigma_{\text{spp}}$.

In contrast, the diagram in Fig. 9(b) represents a physical impossibility: Absence of magnetic charges in nature means that the H -field must be divergence-free everywhere and, in particular, at the metal-vacuum interface; however, since H_{\parallel} will now have opposite directions above and below the surface, it cannot satisfy the requisite boundary condition. This is the reason why SPPs must, of necessity, be TM-polarized.

Conclusion

In this article, we analyzed the surface modes of thin and thick metallic slabs. Maxwell's equations admit many solutions for electromagnetic fields that can be considered localized at and around metallic surfaces (or, in general, confined to the vicinity of metallo-dielectric interfaces). However, only a handful of such solutions extend far enough beyond their point of origination to be considered useful for practical applications. The odd and even waves that propagate along the surfaces of metallic slabs are examples of such long-range surface plasmon polaritons. The remaining solutions—properly classified as short-range or lossy modes—should not be ignored, however, as they participate in the matching of the boundary conditions wherever a long-range SPP is launched, or whenever an existing SPP crosses the boundary from one environment into another.

Our FDTD simulations have verified the validity of the simple theoretical analysis, but they also have provided a

physical picture of field distributions and energy flow patterns in realistic systems that are generally inaccessible to exact mathematical analysis. We have seen, for example, that an SPP excited through a glass prism possesses the expected spatial frequency, but that its decay rate is substantially greater than the theoretical value (due to back-coupling and subsequent leakage through the prism). We also argued that the even mode of a thin metallic slab is less lossy (hence longer range) than the odd mode, primarily because the electrical currents that sustain the even mode flow in the thickness direction, whereas those of the odd mode flow laterally, in the plane of the slab. Much insight can be gained from a detailed analysis of the electromagnetic field profiles in their intimate and intricate relationship with the behavior of the conduction electrons of the metallic medium. \blacktriangle

The computer simulations were carried out using the software package Sim3D_Max, a product of Nonlinear Control Strategies, Inc., Tucson, Ariz. This work has been supported by the AFOSR contracts F49620-03-1-0194, FA9550-04-1-0213, FA9550-04-1-0355 awarded by the Joint Technology Office.

OSA Member [Masud Mansuripur (masud@optics.arizona.edu) is a professor of Optical Sciences at the University of Arizona in Tucson. Arnis Zakharian and Jerome Moloney are with the mathematics department.]

[References and Resources]

- >> J. J. Burke et al. "Surface-polariton-like waves guided by thin, lossy metal films," *Phys. Rev. B* **33**, 5186-5201 (1986).
- >> H. Raether. *Surface Plasmons on Smooth and Rough Surfaces and on Gratings*, Springer-Verlag, Berlin, 1986.
- >> R. D. Averitt et al. "Ultrafast electron dynamics in gold nanoshells," *Phys. Rev. B* **58**, R10203-R10206 (1998).
- >> T.W. Ebbesen et al. "Extraordinary optical transmission through subwavelength hole arrays," *Nature* **39**, 667-9 (1998).
- >> J. J. Mock et al. "Composite Plasmon Resonant Nanowires," *Nano Letters* **2**, 465-9 (2002).
- >> H.F. Ghaemi et al. "Surface plasmons enhance optical transmission through subwavelength holes," *Phys. Rev. B* **58**, 6779-82 (1998).
- >> A. Taflov and S. C. Hagness. *Computational Electrodynamics: The Finite-Difference Time-Domain Method*, 2nd edition, Artech House, 2000.
- >> G. Gay et al. "The optical response of nano-structured surfaces and the composite diffracted evanescent wave model," *Nature Phys.* **264**, 262-7 (2006).